Joachim Landers, Soma Salamon, Samira Webers and Heiko Wende*

Microscopic understanding of particle-matrix interaction in magnetic hybrid materials by element-specific spectroscopy

Abstract: Mössbauer spectroscopy is a well-known technique to study complex magnetic structures, due to its sensitivity to electronic and magnetic interactions of the probed nucleus with its electronic surrounding. It has also been applied to the emerging fields of magnetic hybrid materials as well as to ferrofluids, as information on the magnetic alignment and the velocity of the probed nucleus, i.e. of the particle it is embedded in, can be inferred from the spectra in addition to the above-mentioned quantities. Considering the wide range of preparation methods and sample properties, including fluids, particle powders, sintered pellets, polymer matrices and viscoelastic hydrogels, a considerable advantage of Mössbauer spectroscopy is the usage of y-photons. This allows measurements on opaque samples, for which optical experiments are usually not feasible, also making the technique relatively independent of specific sample geometries or preparation. Using iron oxide nanoparticles in glycerol solution as an exemplary material here, the variety of system parameters simultaneously accessible via Mössbauer spectroscopy can be demonstrated: Spectra recorded for particles of different sizes provided information on the particles' Brownian dynamics, including the effect of the shell thickness on their hydrodynamic diameter, the presence (or absence) and ballpark frequency of Néel superspin relaxation as well as the particles' average magnetic orientation in external magnetic fields. For single-core particles, this resulted in the observation of standard Langevin-type alignment behavior. Mössbauer spectra additionally provide information on the absolute degree of spin alignment, also allowing the determination of the degree of surface spin canting, which limits the maximum magnetization of ferrofluid samples. Analyzing the alignment behavior of agglomerated particles for comparison, we found a completely different trend, in which spin alignment was further hindered by the competition of easy magnetic directions. More complex particle dynamics are observed when going from ferrofluids to hybrid materials, where the particle mobility and alignability depends not only on the particles' shape and material, but also on the matrices' inner structure and the acting force-transfer mechanism between particles and the surrounding medium. In ferrohydrogels for example, particle mobility in terms of

^{*}Corresponding author: Heiko Wende, Faculty of Physics and Center for Nanointegration Duisburg-Essen (CENIDE), University of Duisburg-Essen, Duisburg, Germany, E-mail: heiko.wende@uni-due.de Joachim Landers, Soma Salamon and Samira Webers, Faculty of Physics and Center for Nanointegration Duisburg-Essen (CENIDE), University of Duisburg-Essen, Duisburg, Germany

Mössbauer spectroscopy was probed for different crosslinker concentrations, resulting in widely different mesh-sizes of the polymer network and different degrees of freedom. While a decrease in particle dynamics is clearly visible in Mössbauer spectroscopy upon rising crosslinker density, complementary AC-susceptometry experiments indicated no Brownian motion on the expected timescales. This apparent contradiction could, however, be explained by the different timescales of the experiments, probing either the relatively free Brownian motion on ultrashort timescales or the more bound state preventing extensive particle motion by interaction with the trapping mesh walls in the millisecond regime. However, it should also be considered that the effect of the surroundings on particle rotation in AC-susceptometry may also differ from the variation in translational motion, probed by Mössbauer spectroscopy. Being sensitive mainly to translational motion also results in a wide range of particles to be accessible for studies via Mössbauer spectroscopy, including larger agglomerates embedded in polymers, intended for remote-controlled heating. Despite the agglomerates' wide distribution in effective diameters, information on particle motion was found to be in good agreement with AC-susceptometry experiments at ultralow frequencies in and above the polymer melting region, while additionally giving insight into Néel relaxation of the individual nanoparticles and their magnetic structure.

Keywords: Mössbauer spectroscopy, nanoparticle dynamics, nanoviscosity, relaxation phenomena

1 Introduction

Mössbauer spectroscopy is an element-specific and non-destructive absorption technique, based on the effect of resonant nuclear absorption of γ -rays, discovered by Rudolf Mößbauer in 1958 [1]. Due to its ability to characterize a material's "fingerprint" hyperfine structure, it was established as a key technique in the fields of materials science, magnetism and molecular studies and even led to significant discoveries in geology, astrophysics and archeology [2–5].

In addition to one of its primary usages in the analysis of static magnetic properties, including phase composition, iron site occupation [6] and magnetic alignability, Mössbauer spectroscopy was found to exhibit several properties that make it a versatile technique for the study of magnetic hybrid materials (see also chapter 2):

While there are several methods to access nanoparticle dynamics on the macroscopic scale, Mössbauer spectroscopy provides information on very local properties in combination with very short timescales. Thereby, one can yield valuable insight into the field of nanoviscosity, i.e. how the nanostructure of the surrounding medium affects the (sub-) diffusive behavior of magnetic nanoparticles (MNPs) on different time- and length scales.

- As it is sensitive to the dynamics of individual atomic magnetic moments instead of a macroscopic net magnetization, Mössbauer spectroscopy is able to clearly distinguish between different magnetic relaxation mechanisms. As will be illustrated in more detail below, this can be utilized to characterize Néel-type relaxation and Brownian motion separately, studying either the characteristic deformation of the spectrum affected by the frequency of internal reorientation of the particles' superspin or the symmetric broadening of the absorption lines evoked by the Doppler effect corresponding to diffusive nanoparticle Brownian motion.
- In combination with standard magnetometry, optical experiments belong to the most frequently used approaches for the characterization of MNPs in ferrofluids. In the case of higher nanoparticle concentrations or for the study of MNPs in solid matrices, this approach may not be feasible. Mössbauer spectroscopy utilizes y-radiation in the keV-range (14.4 keV for the most common isotope ⁵⁷Fe), yielding appropriate penetration depths of ca. 5-15 mm for common matrix materials (water-based ferrofluids, hydrogels, polymer matrices), the latter being dependent on the density and atomic number of the used elements, being similar for the above-mentioned examples. Thereby, samples of sufficient iron concentration can be studied in detail relatively independent of their thickness and type of preparation (powder, fluid, solid), without being hindered by opaque matrix materials.
- Although less often applied in the preparation of magnetic hybrid materials, paramagnetic, superparamagnetic or antiferromagnetic (nano-) particles may resist the most commonly used magnetometry experiments for sample characterization. Mössbauer spectroscopy allows the analysis of such materials as well, due to its sensitivity to the interactions between the active nuclei und their electronic surroundings.

Based on these favorable properties, Mössbauer spectroscopy was applied to ferrofluids relatively soon after its invention, early studies being performed for example by Bhonchev et al. [7, 8], supported by a theoretical description on the influence of different types of diffusive motion on the spectral structure by Singwi and Sjölander [9]. Beside iron-based nanoparticles in fluids, as ferrofluids were a less intensively studied field back then, Mössbauer studies on diffusive processes included the atomic diffusion of ⁵⁷Fe atoms in crystal lattices [10, 11], molecular dynamics [12, 13] and even diffusive processes in nature [14]. In recent years, it has also been applied to magnetic nanoparticles in hydrogels, gels, polymer compounds, porous media and even liquid crystal systems [15–17].

To provide an overview over possible ways to apply Mössbauer spectroscopy, what has to be considered in the evaluation of experimental spectra and which quantities can be extracted from it, several examples will be given in chapter 3-5 including temperature-dependent as well as in-field experiments on ferrofluids, hydrogels and magnetic polymer compounds. The required theoretical background regarding the

basics of Mössbauer spectroscopy and the different apprehended spectral features are presented in chapter 2.

2 Theoretical background

Mössbauer spectroscopy is a non-destructive measurement method based on the nuclear resonant emission and absorption of γ -photons. For atoms incorporated into crystalline solid bodies, there is a certain probability (given by the Lamb-Mössbauer factor, also called Debye-Waller factor) for such a photon to be emitted recoil-free, without the change in emission energy associated with the generation of phonon lattice vibrations, as well as for the same photon to be absorbed again by another ⁵⁷Fe nucleus, referred to as resonant emission and absorption [2].

In the most commonly used standard transmission setup shown schematically in Figure 1(a), the radiation source, often consisting of paramagnetic 57 Co atoms embedded in a metal foil (e.g. Rhodium), is mounted on an electromechanical Mössbauer drive, which oscillates the source back and forth, in order to modulate the emitted γ -photon energies via the optical Doppler effect. The sample is placed behind the radiation source, with the distance being dictated by the avoidance of too small spacings that would lead to angular dependent effects (so-called "cosine smearing"), or excessively large spacings, which would lead to a diminished number of photons arriving at the sample. Once having passed through and interacted with the sample, the remaining γ -photons are recorded by a detector, e.g., a proportional counter. Other types of Mössbauer spectroscopy include synchrotron setups, measurements in backscattering geometry or the detection of conversion electrons, each with its different advantages, as, e.g., enhanced surface sensitivity [18].

These 14.4 keV γ -photons are emitted after the decay of 57 Co source atoms to 57 Fe, when relaxing from the excited I=3/2 57 Fe nuclear state to the ground state. According to Heisenberg's uncertainty principle, the first excited nuclear state's relatively long half-life of 98 ns corresponds to a narrow natural linewidth of the emitted γ -radiation of less than 5 neV, being the origin of the method's extreme energy resolution. This enables the investigation of miniscule variations in absorption energy of the studied 57 Fe atoms, caused by the so-called hyperfine interactions between 57 Fe nuclei and the surrounding electrons. The effects most frequently discussed in the study of static magnetic properties are the isomer shift δ , i.e. the shift of the entire spectrum relative to a reference material, the nuclear Zeeman splitting quantified by the hyperfine magnetic field B_{hf} , causing the characteristic sextet line structure in case of magnetically ordered samples, and the quadrupole splitting ΔE_Q (or nuclear quadrupole level shift 2ε), see Figure 1.

When studying a magnetically ordered sample in an external magnetic field, there are two primary effects giving insight into the magnetic behavior of the material: The change in nuclear Zeeman splitting caused by the superposition of the internal

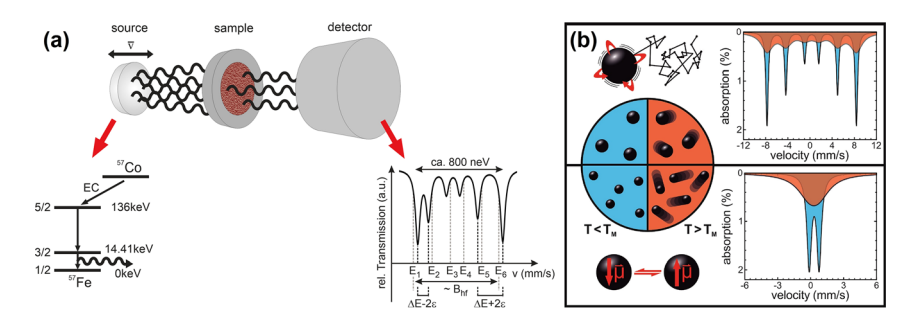


Figure 1: (a) Schematic illustration of nuclear energy-levels following the decay of 57 Co source material generating highly monochromatic γ-radiation and contributions to hyperfine structure, and (b) the effect of different relaxation mechanisms on the Mössbauer spectrum for small particles (Néel relaxation, bottom) and large particles (top) in rigid (left) or liquid matrices (right, broadened lines), adapted with permission from [19], Copyright (2016) American Chemical Society.

"hyperfine field" B_{hf} and the external magnetic field B_{appl} , and the variation in relative line intensities, in accordance to absorption probabilities of dipole radiation dependent on the angle between spin and the direction of the incident γ-photon, given by Fermi's golden rule. The first one can be determined directly as vectorial sum of B_{hf} and B_{appl} , leading, e.g. to a reduction of sextet splitting in ferromagnets, as B_{hf} is antiparallel to the iron atoms' magnetic moment, while the latter is often characterized by the so-called A_{23} line ratio as given in Eq. (2.1) dependent on the average spin canting angle θ between spin and γ-photon direction [20, 21]. This is also illustrated in detail for in-field Mössbauer spectra in chapter 3.2.

$$A_{23} = \frac{I_2}{I_3} = \frac{4\sin^2(\theta)}{1 + \cos^2(\theta)}$$
 (2.1)

The parameter A_{23} is therefore a representation of the average magnetic alignment of the system, dependent on the applied field amplitude and can thus be understood as comparable to a single data point in a standard field-dependent magnetometry experiment. However, A_{23} exhibits a fundamental difference, as it provides an absolute measure of magnetic orientation, a distinction that is most obvious, e.g., in the study of magnetic nanoparticles, often reported to have a reduced saturation magnetization M_S due to frustrated surface spins or reduced magnetic moments in the top atomic layers [22]. This expression "saturation magnetization" has to be considered with caution, as nanoparticle samples seemingly being saturated may exhibit values of A_{23} far from 0, a clear indication that in such systems the "reduction" in M_S can primarily be assigned to spin frustration instead of reduced magnetic moments, whereby the term "high-field magnetization" may be more appropriate instead.

In terms of magnetic hybrid materials, the time constants of Mössbauer spectroscopy are also of interest, i.e. the Larmor precession frequency (e.g. $\omega_{Larmor} \approx 200 \text{ MHz} \rightarrow \tau_{Larmor} \approx 5 \text{ ns}$ for $B_{hf} \sim 50 \text{ T}$) and the half-life of 98 ns, making the

technique highly sensitive to magnetization dynamics on the nanosecond timescale. Thereby it is a valuable extension of the more commonly used approaches on soft magnetic hybrid systems via rheology or susceptometry experiments etc., as these usually work on the range of seconds to microseconds.

The thermally excited relaxation of a nanoparticle's magnetic moment (Néel superspin relaxation), present in case the thermal energy begins to overcome the magnetic anisotropy energy barrier of the particle, will lead to a reduction in sextet splitting when approaching the timescale of τ_{Larmor} , on which we observe the timeaveraged nuclear Zeeman splitting [23]. Combined with lognormal distributions of particle core diameter and anisotropy energy characteristic for the result of nanoparticle growth processes, this will create easily recognizable asymmetric lineshapes, as different Néel relaxation times will result in almost unchanged values of B_{hf} for larger particles and strongly reduced ones for smaller particles, finally reaching the completely superparamagnetic doublet state [24, 25]. By using an adequate relaxation model as proposed e.g. by Blume et al. [26] or more complex many-state relaxation models [27, 28], one can reproduce the variation in lineshape and the degree of sextet collapse into the doublet state to extract the magnetic anisotropy energy of the particles, including effects of interparticle interaction decelerating Néel relaxation [29, 30].

Brownian particle motion, on the other hand, has a completely different effect on the spectral structure. As it introduces an additional relative instantaneous velocity between the absorbing ⁵⁷Fe atom and the ⁵⁷Co source, the diffusive motion also corresponds to a Doppler shift of the absorption energy, or, as the measured spectrum is averaged over a long time and a huge ensemble of particles moving statistically in all directions with the same probability, it leads to a Doppler broadening $\Delta\Gamma$ of the absorption line. The latter is proportional to the velocity of an absorbing atom, mainly generated by translational diffusion of the particle the 57Fe atom is embedded in, as described in Eq. (2.2) [9]. Here, k denominates the wave vector corresponding to the y-photon energy of 14.4 keV, D_T the translational diffusion coefficient, η the carrier fluid's dynamic viscosity, T the temperature and R_H the particle's hydrodynamic radius. Minor contributions to atomic motion are also caused by nanoparticle rotation, which is, however, seldomly studied in detail [31] and often neglected in first approximation calculations.

$$\Delta\Gamma = 2\hbar k^2 D_T \propto \frac{T}{R_H \eta} \tag{2.2}$$

With the half-life of only 98 ns, corresponding to the natural linewidth of ca. 5 neV or a half-width of 0.085 mm/s in the Mössbauer spectrum, a line broadening induced by Brownian particle motion may be detected being as small as 0.01 mm/s, yielding diffusion coefficients in the range of 10^{-16} – 10^{-17} m²/s, while linewidths up to several 100 mm/s have also been studied in case of sufficient spectral area (intensity). Thereby being sensitive to particle motion on the nanosecond timescale (corresponding to equally small length scales the particle is covering in these few nanoseconds), [32] Mössbauer spectroscopy is, although applicable to Fe-bearing particles in liquids, even more promising for the study of magnetic hybrid materials. For these, short-time particle-matrix interactions may define the materials' behavior in terms of particle mobility and magnetic alignment. This statement is further reinforced by the fact that the probed motion is the component of particle diffusion along the y-ray propagation direction, as atomic velocities in other directions do not contribute to the detected linear Doppler effect. Thereby even measurements of direction-resolved diffusion coefficients are in principle possible [33, 34], especially interesting for the study of either strongly elongated nanoparticles or the dynamics of particles in anisotropic nanostructures [35, 36]. In addition to the broadening of the absorption lines, Brownian motion also affects the probability for resonant absorption, usually described in terms of the Debve-Waller- or Lamb-Mössbauer factor f. Similar to lattice vibrations or molecular dynamics, accelerating diffusive motion will result in a decrease in resonant absorption for the benefit of quasi-elastic contributions. [37] However, due to the different timescales involved in the above-mentioned processes and further differences - does the atom perform free motion, bound diffusion or purely vibrational dynamics? - the dependence of resonant absorption on the covered mean square displacement of the ⁵⁷Fe nucleus will strongly depend on the specific mechanism and material at hand [13, 38, 39].

3 Accessing nanoparticle dynamics

3.1 Simultaneous determination of Néel and Brownian dynamics in ferrofluids

To obtain a general overview on particle magnetization dynamics studied via Mössbauer spectroscopy, we will start by looking at monodisperse nanoparticles in a Newtonian fluid, minimizing the number of further parameters apart from the beforementioned theory. Commercial ferrofluidic samples were used (Ocean NanoTech SHP-series), which we denote with regard to the used nanoparticles as S(mall), M(edium) and L(arge), as the contained iron-oxide nanoparticles were spherical in shape, with core diameters of 6.0, 14.8 and 26.4 nm. The particles were coated with an amphiphilic polymer and oleic acid and dispersed in 70 vol% glycerol solution. For Mössbauer experiments ca. 500 µl of each ferrofluid were used, to ensure sufficient spectral intensity. Due to the nanoparticle concentration of ca. 1.5 wt%, the absorption signal was relatively small compared to a common Mössbauer experiment on powder samples. Ca. 50 µl were used for complementary magnetometry and AC-susceptometry experiments.

As the nanoparticles used in sample S-L cover a wide range of core diameters (Figure 2(a)), going from predominant Néel superspin relaxation in the smallest particles to blocked Néel relaxation in larger ones, leaving Brownian motion as only mechanism

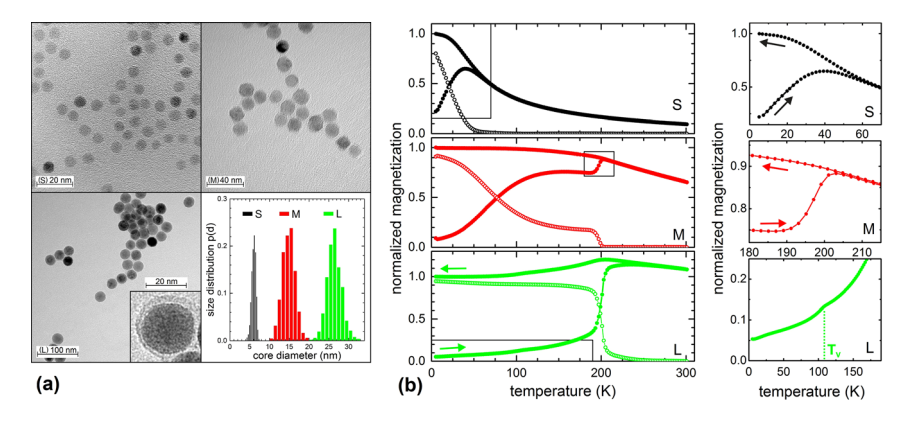


Figure 2: (a) TEM images and size distribution analysis, and (b) ZFC-FC magnetometry of ferrofluid samples S–L. The images verify the regular spherical shape as well as particle monodispersity. Temperature-dependent magnetometry demonstrates different magnetization dynamics, dominated by either the Néel (S) or the Brownian mechanism (L), or the combination of both (M). Focus regions of interest (right-hand side) are shown in magnification, i.e. Néel blocking temperatures (S), the onset of Brownian motion (M) and the Verwey transition at T_V (L), proving the presence of magnetite (particle core) material. Adapted with permission from [19], Copyright (2016) American Chemical Society.

for magnetic reorientation, temperature-dependent magnetometry already provides valuable reference information on magnetic dynamics. Here, the standard ZFC-FC methodology was applied, where the temperature-dependent magnetization is measured after cooling down the sample either without (zero-field-cooled) or with a minor external magnetic field (field-cooled), where a change in the splitting between both curves represents the onset of magnetic realignment processes, whereby identical curves M_{ZFC} and M_{FC} indicate the completely superparamagnetic state [40, 41]. The results of these experiments shown in Figure 2(b) display Néel-type blocking temperatures of ca. 20–30 K for sample S and ca. 80–100 K for sample M. Also, a relatively sharp increase in magnetization is visible at ca. 200 K, marking the onset of Brownian motion, allowing the reorientation of all previously blocked (large particle) magnetic moments in field direction on the timescale of the magnetometry experiment [42]. Similar behavior is seen at ca. 200 K for sample L, although here almost all magnetic moments are blocked at lower temperatures due to the larger particles' higher anisotropy energy E_A .

Although the observation of a superparamagnetic state depends on the time-scale of the experimental technique at hand, which is of course very different in magnetometry (seconds to hours) and Mössbauer spectroscopy (nanoseconds), this precharacterization provides valuable insight and goes hand in hand with the observed general structure of the corresponding Mössbauer spectra visible in Figure 3. As has been found in a similar manner in studies on Néel relaxation in powder samples of small nanoparticles in sample S, we find a state of fast Néel relaxation (presumably the relaxation frequency is comparable to the Larmor frequency), where the sextet

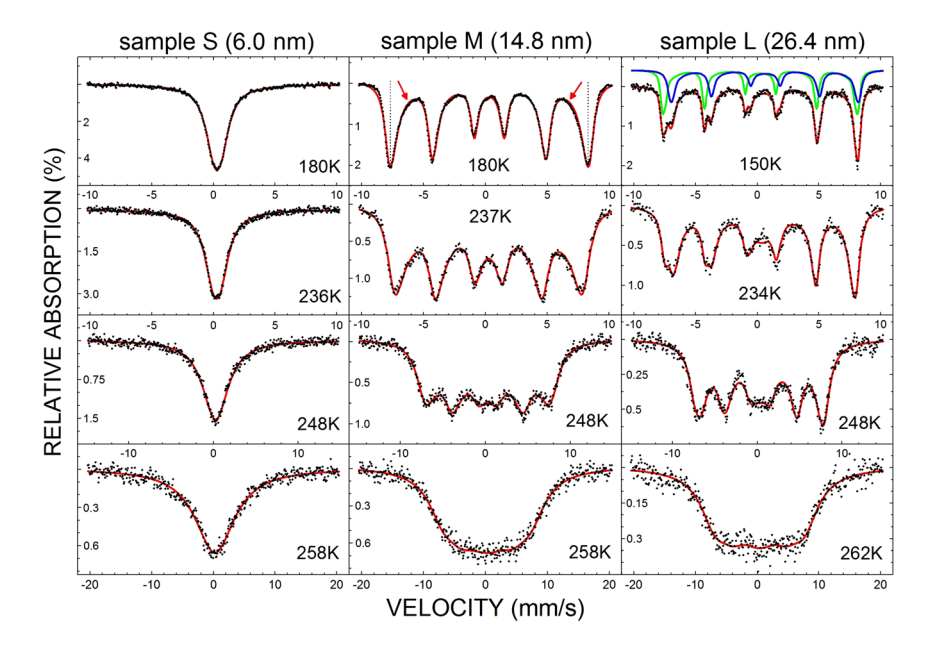


Figure 3: Mössbauer spectra of ferrofluid sample S–L recorded upon rising temperature at 234–262 K. Reference (static) Mössbauer spectra measured at 150–180 K are shown on top, which were used to extract trends in hyperfine parameters for the modeling of the spectra affected by Brownian line broadening. Reprinted with permission from [19], Copyright (2016) American Chemical Society.

structure has already collapsed, while the doublet structure of the "completely" superparamagnetic state is still obscured. The largest particles in sample L on the other hand display almost no sign of spin dynamics, showing more or less symmetric absorption lines, which allows us to assign subspectra positions corresponding to ⁵⁷Fe on the lattice sites of tetrahedral (A-site, green) and octahedral geometry (B-site, blue). Particles of intermediate core diameter (sample M) exhibit absorption lines with a characteristic asymmetric deformation, from which the distribution of anisotropy energies can be extracted using an appropriate theoretical model [28]. Comparing common magnetic characterization techniques, at this point the major difference between Mössbauer spectroscopy on the one hand and magnetometry and susceptometry on the other hand becomes evident: ZFC-FC magnetometry experiments display at which temperature a change in particle dynamics takes place, allowing only indirect deduction on the relevant parameters, and AC-susceptometry provides the total relaxation frequency of present relaxation mechanisms. Mössbauer spectroscopy on the other hand, while less direct in data evaluation, allows the simultaneous extraction of Néel as well as Brownian parameters (anisotropy energy E_A , diffusion coefficient D_T), as these processes affect different features of the Mössbauer spectrum [19, 43].

Now focusing on particle diffusion in the three ferrofluids, we extract the Brownian line broadening from the spectra. Regarding the spectra at rising temperatures, beginning at ca. 230–240 K, we see that the broadening of the lines becomes evident. In order to determine the line broadening and thereby nanoparticle diffusion coefficients, we have to reproduce the spectral structure with an appropriate fitting model and subtract the static linewidth Γ_{stat} from the total linewidth Γ . Therefore, the information on Brownian dynamics cannot be determined from the spectra without considering the influence of Néel relaxation on the lineshape and recording e.g. a reference spectrum at sufficiently low temperature, where the solid carrier medium does not allow Brownian motion and cancels the additional Doppler broadening of the absorption lines (providing Γ_{stat}). Alternatively, if the carrier fluid does not crystallize but instead exhibits a glass transition, as in the case presented here using glycerol solution, Γ_{stat} could also be extrapolated from spectra at sufficiently low temperatures (ultrahigh viscosities), where Doppler broadening is present but far smaller than the static linewidth [44, 45].

The particle diffusion coefficient can now be estimated by usage of Eq. (2.2) from the temperature-dependent line broadening shown in Figure 4(a). The same goes for the dynamic viscosity of the carrier medium in Figure 4(b) under the consideration that hydrodynamic diameters are known. The three particle core diameters present in sample S, M and L yield identical trends in η (T) assuming an effective coating thickness of ca. 5 nm, the latter being in good agreement with coating thicknesses reported by the manufacturer [19]. Since the glycerol solution used as carrier medium is a simple Newtonian fluid, unlike in experiments discussed later on, where effects of nanoviscosity have to be considered, the agreement between the dynamic viscosity η (T) obtained via Mössbauer spectroscopy with that determined in macroscopic rheological experiments from literature proves the applicability of the presented approach for the study of particle diffusion [46].

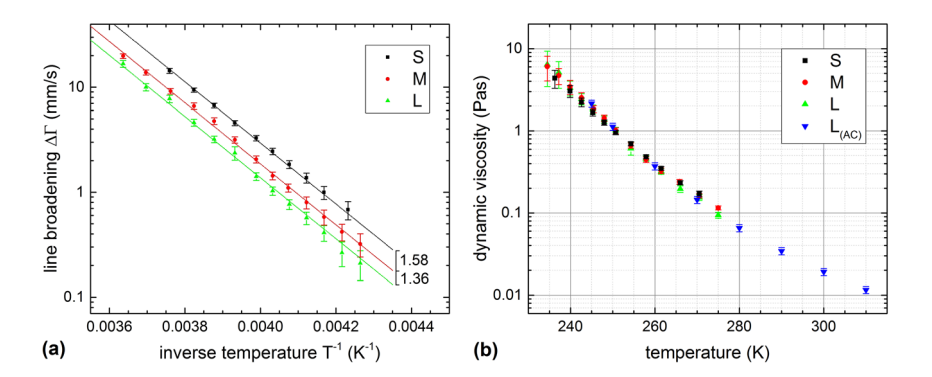


Figure 4: (a) Doppler line broadening of sample S–L extracted from Mössbauer spectra, with factors 1.58 and 1.36 originating from the different values of R_H in the ferrofluids, and (b) derived values of the carrier fluid's dynamic viscosity. Adapted with permission from [19], Copyright (2016) American Chemical Society.

3.2 Dynamics of nanoparticle agglomerates in polymer melts

Brownian particle dynamics are also studied for agglomerates in polymer melts, representing a system with similarities, as well as differences to the spherical particles in glycerol solutions discussed above. This gives us the opportunity to compare particle dynamics in Mössbauer spectroscopy on different scales of effective particle diameter and dynamic viscosity. The biopolymers used here are based on meltable dextran ester, designed to allow on-demand drug release through internal heating via the embedded nanoparticles when exposed to an AC-magnetic field [47, 48]. While the particles are of ca. 15 nm in diameter, it has to be considered that in the as-studied biopolymer composite material, a fraction of particles forms larger 30-80 nm multicore agglomerates that have a larger specific heating power than smaller superparamagnetic nanoparticles [49].

Therefore, despite the relatively high hydrodynamic particle diameter, Néel relaxation of the individual particle superspins has to be considered in the modeling of the experimental spectra as shown in Figure 5(c, d), recorded at temperatures between room temperature - below the polymer melting region - and temperatures of ca. 120 °C. Here, one observes similar relaxation features as for the above-mentioned intermediate sized particles in sample M. One should keep in mind that, when discussing effective anisotropy barriers, magnetic dipolar interaction between neighboring particles in agglomerates discussed here may be a considerable contribution, which can usually be neglected in ferrofluids of low MNP concentration [50].

In terms of Brownian motion, the rather high viscosity of the polymer melts of ca. 30–1 Pas in the temperature region of 55–100 °C in combination with the high effective diameters leads to far lower line broadening as compared to the ferrofluidic samples. At this point, size distribution effects have to be introduced for the first time, affecting the agglomerate (effective hydrodynamic) radius R_H much more than the relatively narrow core diameter distribution. As the main component of the Doppler line broadening is caused by translational Brownian motion, this line broadening can be considered as proportional to R_H^{-1} , with the signal intensity of agglomerates being directly dependent on the number of included ⁵⁷Fe-atoms, whereby the number distribution of hydrodynamic diameters has to be weighted with the particle volume when being applied to reproduce spectral features. To some extent, the distribution P(D_H) can be extracted from the measurement by adding a distribution of linewidths to the spectrum, while utilizing fixed hyperfine parameters that were extrapolated from low temperature measurements. In agreement with the line broadening from spectra shown in Figure 5(c, d), an average effective agglomerate diameter of ca. 64 nm was found in AC-susceptometry measurements [51].

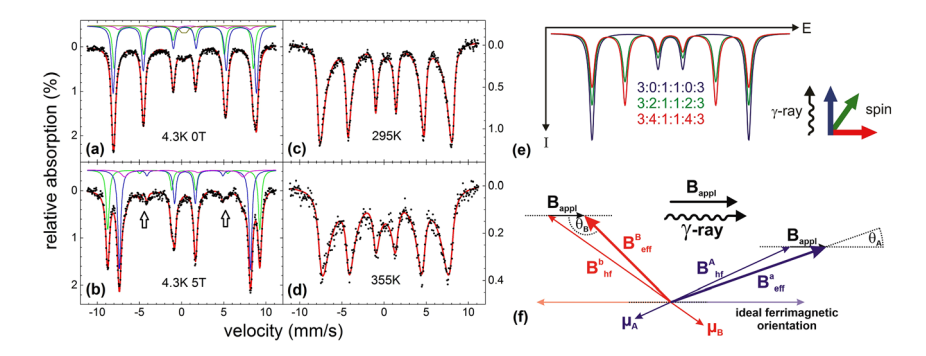


Figure 5: Mössbauer spectra of iron-oxide nanoparticles in biopolymers at 4.3 K with (b) and without (a) an external magnetic field of 5 T, at room temperature (c) and in the molten polymer state at 355 K (d), reprinted from [51], Copyright (2016), with permission from Elsevier. Arrows in (b) mark lines 2 and 5, whose relative intensity is determined by the average angle θ between spin and γ -ray propagation direction, as illustrated in (e), (f) effective magnetic fields in ferrimagnetic materials, adapted with permission from [20]. For symmetry reasons, usually the canting angles are given relative to ideal ferrimagnetic orientation in spinels, yielding values of 0–90° [52].

Additional information on the composite material was obtained from Mössbauer experiments performed at cryogenic temperatures of 4.3 K with (b) and without (a) an external magnetic field of 5 T along the γ -ray propagation direction (Figure 5). At such low temperatures there is no additional line broadening either by Néel relaxation or by Brownian diffusion, wherefore fine structures of the spectrum can be studied more easily, allowing the resolution of individual contributions of B-site Fe³⁺(blue), B-site Fe²⁺ (violet) and A-site Fe³⁺ (green) due to their minor differences in isomer shift, hyperfine magnetic field B_{hf} and quadrupole splitting [29]. From the relative amount of Fe²⁺ ions (ca. 9%), the magnetite fraction in the nanoparticles can be estimated to roughly 25–30%, indicating a core of original magnetite material remaining from the as-synthesized state, surrounded by an oxidized maghemite passivation layer, slowing down further oxidation [53, 54]. A minute doublet in Figure 5(a) could indicate a minor paramagnetic contribution in the particles; the existence of a superparamagnetic doublet at such low temperatures is unlikely due to the minimum thermal energy at 4.3 K.

By applying an external magnetic field, we can also determine the total degree of particle magnetic alignment for each component and even the sublattices individually by comparing the relative sextet line intensities and using Eq. (2.1). By this method, we can extract canting angles of ca. 15° for the A-site and ca. 21° on average relative to ideal ferrimagnetic alignment for Fe²⁺ and Fe³⁺ on octahedral lattice positions from the in-field spectrum. In Figure 5(b) one can clearly see the shift of the tetrahedral A- and octahedral B-site subspectrum into different directions via the superposition of the external field $B_{appl} = 5$ T and the hyperfine magnetic fields $B_{hf,(4,3)} \approx 50-52$ T, which are antiparallel for A- and B-site due to the material's ferrimagnetic structure, as showcased in Figure 5(f).

It is important to keep in mind that, although the spectrum shown in Figure 5(a) recorded at 4.3 K is helpful for the general characterization of the nanoparticle component of composite materials, it should not be used as a reference for the determination of line broadening in spectra above room temperature, deviating in hyperfine parameters as well as Néel relaxation due to temperature effects. For that purpose, instead a spectrum should be utilized, which was measured at only slightly lower temperatures, where the spectral structure is almost identical, while Brownian motion is still slow enough to create negligible line broadening, as visible e.g. through comparison of spectra (c) and (d) of Figure 5.

4 Magnetic alignment and dynamics: comparison of individual MNPs and NP-agglomerates

In the first section of the previous chapter we discussed the simultaneous analysis of individual magnetic relaxation processes (Néel relaxation and Brownian particle motion), while in the following section the method to study magnetic particle alignment via Mössbauer spectroscopy was introduced. Although the latter is more commonly applied in the study of static magnetic properties in solids, the change in the nanoparticles' magnetic orientation as a response to an external stimulus (magnetic or electric fields, matrix deformation, temperature change, etc.) can also be probed in fluid or viscoelastic hybrid materials. This is demonstrated in the following, by probing the superspin orientation in ferrofluidic samples in combination with the particles' Brownian dynamics as well as Néel relaxation. We will see that by the combination of the field-dependence of these quantities, we can also infer properties such as surface spin canting and the presence and size of nanoparticle agglomerates in the fluids.

Samples of the original ferrofluids S and M as introduced in chapter 3.1 were used for this in-field Mössbauer study, in combination with a newly prepared sample L, with a core diameter of 22.0 nm similar to the original sample [55]. To obtain a thorough and precise measurement of the magnetic orientation, spectra as shown in Figure 6 were recorded in external magnetic fields parallel as well as perpendicular to the y-ray propagation direction, by using either an electromagnetic coil setup (maximum field ca. 1 T) or a set of permanent NdFeB ring magnets, providing homogeneous fields without blocking the y-pathway (see Figure 6, schematic setup). Upon rising temperature, the exponential increase in linewidth leads to some superposition of the sextet of absorption lines. Still, up to a maximum linewidth of ca. 2–3 mm/s the variation in relative line intensities induced by the external magnetic field is visible even by eye, while at linewidths larger than 5–10 mm/s, the estimation of the parameter A_{23} is less precise even using professional modeling software. In parallel field geometry a decrease, and in perpendicular geometry an increase in A_{23} is visible, corresponding to the same trend of increasing magnetic alignment probed from two different directions,

leading to lower, respectively higher angles between probing γ -ray and field (and preferred nanoparticle magnetic moment) direction. In these spectra, no distinct splitting between A- and B-site spinel subspectra is observable as it was in an external magnetic field of 5 T as shown in Figure 5. Although sufficient to align the magnetic nanoparticle moments in our ferrofluidic samples, the field amplitude of up to ca. 0.2 T is too small to lead to a clearly visible variation in relative line positions of the subspectra. Sample M exhibits some beginning Néel relaxation, leading to the characteristic asymmetric lineshapes, as was visible in Figure 3, apart from which it displays similar changes of spectral structure as in-field experiments on sample L do in Figure 6.

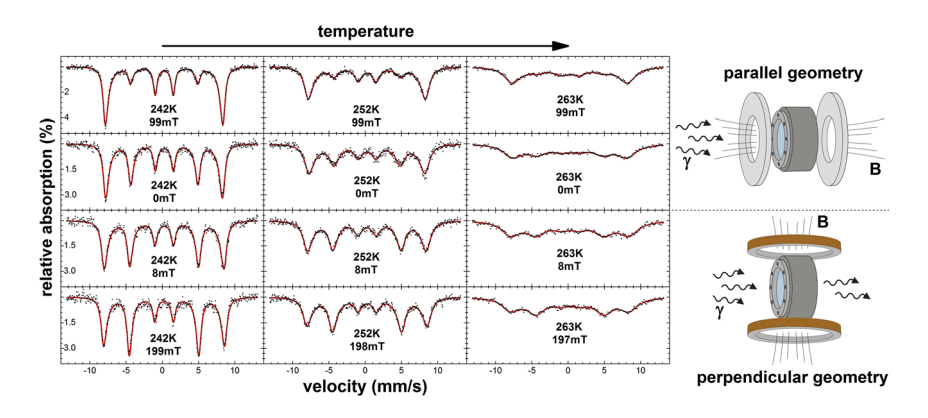


Figure 6: Mössbauer spectra of ferrofluid L recorded at 242–263 K in external magnetic fields of up to 199 mT applied either perpendicular (bottom) or parallel (top) to the γ -ray propagation direction, as illustrated in the adjacent schematic setups. Reprinted with permission from [55], Copyright (2019) American Chemical Society.

Values of A_{23} are displayed in Figure 7(a) against the rising magnetic field amplitude for intermediate sized particles in sample M. As discussed above, here the two clear branches represent the increasing degree in nanoparticle in-field alignment probed from two different directions, where $A_{23}=4$ would match a spin alignment perpendicular to the γ -ray propagation and $A_{23}=0$ coaxial (antiparallel) spin and γ -direction. Both branches start at $A_{23}=2$, representing a 3D-random distribution of spin directions as expected of an ensemble of single-domain magnetic nanoparticles in a ferrofluid in the absence of external fields. Although we approach the maximum and minimum A_{23} -values mentioned above, the trend in A_{23} (H) clearly does not converge completely in the covered range of field amplitudes. Seemingly both branches A_{23} (H) converge towards lower degrees of ordering, caused by a minor degree of nanoparticle surface spin canting. We assume the degree in surface spin frustration to change moderately for different magnetic fields, whereby it would produce an almost constant background in Figure 7(a), defining the maximum attainable spin alignment before going to much higher field amplitudes.

Based on these considerations, $A_{23}(H)$ is theoretically reproduced using standard Langevin theory to describe the distribution of superspin orientations in an external magnetic field at a given temperature. To consider spin frustration at the particle surface, the Langevin model function is weighted with (1-x), with x being the fraction of canted surface spins, added to $2 \cdot x$, as the frustrated spin fraction is assumed to be random in orientation (with $A_{23} = 2$). This model yields excellent agreement to experimental data, describing the first two regions of A_{23} (H) as shown in the insets of Figure 7(a): The low-field range I, where the random distribution of superspins yields $A_{23} \approx 2$, and the intermediate-field range II, where the superspins are primarily aligned, with a remaining degree of spin disorder from frustrated surface layers. In these two regions, the model yields a net magnetic moment of 6.6·10⁻¹⁹ Am² for the alignable nanoparticle core moment in sample M, and a fraction of frustrated surface spins of ca. 13%. Combining these two parameters, the saturation magnetic moment of the particles is in the range of 7.6·10⁻¹⁹ Am², in good agreement with estimations based on the maghemite bulk saturation magnetization and the particles' average volume. This total magnetic moment corresponds to a state of complete spin alignment, which is however attainable only for much higher fields (range III), starting also the (partial) alignment of surface moments, and is thus not feasible in our experiment. It is worth noticing that although values of A_{23} were extracted from spectra measured in a broad temperature interval with values of $\Delta\Gamma$ ranging from ca. 0.2–5 mm/s, no significant deviations in the extracted line ratios are observable, proving that this approach can be reproduced for samples of different particle mobility.

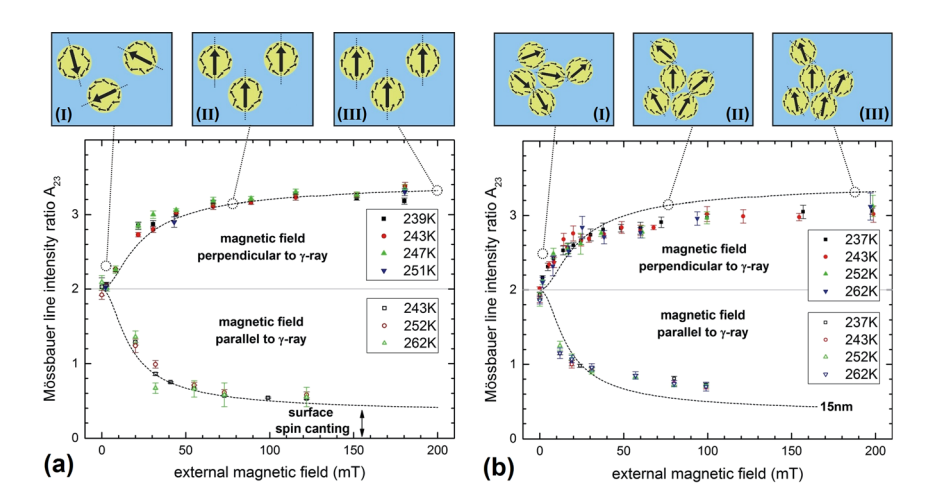


Figure 7: A_{23} line intensity ratio versus external magnetic field in perpendicular (top) and parallel field geometry (bottom) for ca. 15 nm particles in sample M (a) and larger 22 nm particles in sample L (b), evaluated at several temperatures at 237–262 K. Dashed lines represent the modeled trend in A_{23} (H) for sample M corresponding to the modified Langevin approach describing field- and temperature-dependent magnetic alignment. Adapted with permission from [55], Copyright (2019) American Chemical Society.

One could notice that the experiment effectively provided the particles' net magnetic moment via the Langevin parameter, which is also available by standard field-dependent magnetometry. As long as this parameter is the only quantity required, this is a correct statement. However, if a more thorough sample characterization is needed, this approach provides, as illustrated above, not only a total measure of spin alignment, but also the ability to characterize the particles' static magnetic structure, magnetization dynamics and orientation simultaneously from one spectrum or at least one series of experiments.

While results obtained on sample M were found to be in good agreement to theoretical models designed to describe spin and superspin alignment of isolated particles in ferrofluids exposed to magnetic fields, a different behavior is observed for larger particles in sample L, shown in Figure 7(b). In the low-field region the degree of particle alignment rises much faster as compared to sample M (dashed line), while above ca. 30 mT sample L shows either a slower convergence to a saturation state or a lower final degree of spin orientation. As experimental data of A_{23} (H) for both samples display a crossing at ca. 30 mT, we can deduce an additional effect to be present, as a variation in particle core diameter and net magnetic moment will affect the Langevin parameter but will never create a crossing. Additional information was taken from spectra of sample L (Figure 6), leading to an average hydrodynamic diameter R_H of ca. 68 nm estimated from the absorption line broadening. Since the original sample L, as discussed in Section 3 consisted of individual monodisperse nanoparticles, this indicates nanoparticle agglomeration in the second batch of sample L.

Based on the assumption of small particle agglomerates, their net magnetic moment was extracted by modeling only the low-field region of A_{23} (H) and M (H), where the relatively high agglomerate net magnetic moment is expected to yield high Langevin parameters and spin alignment. At the same time, the field is low enough to ensure not to increase the net magnetic moment by aligning the individual particle superspins out of their preferred direction defined by magnetic anisotropy. Comparing agglomerate magnetic moments from this approach and estimated magnetic moments of individual 22 nm particles, and also taking into account the agglomerates' saturation moment extracted from the high-field region in M(H), we estimate an average number of 8–22 particles per agglomerate. This translates to an effective hydrodynamic diameter of 64–90 nm, matching estimations made based on the line broadening (68 nm) and from AC-susceptometry (77 nm).

With the comparison of sample M and L leading to exciting insights regarding alignment behavior and agglomeration, it seems reasonable to perform a similar attempt for sample S. Here, the small anisotropy energy of the particles with only 6.0 nm core diameter results in a completely superparamagnetic doublet spectrum, from which the line broadening, i.e. particle dynamics, but no longer the line intensity ratio, i.e. spin orientation, can be inferred. Still, a rough estimation is possible when going to higher fields of >300 mT, where the external field deforms the anisotropy

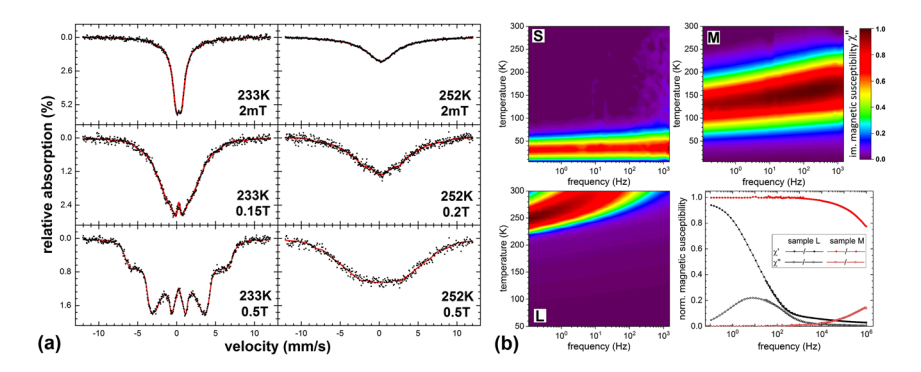


Figure 8: (a) Mössbauer spectra of 6.0 nm particles in sample S recorded in perpendicular field geometry up to 0.5 T and temperatures of 233–252 K, (b) colorplots of the imaginary part of magnetic susceptibility χ'' measured for sample S–L at 5–300 K and 0.1–1500 Hz, also measured on a wider frequency scale for samples M and L at room temperature. Adapted with permission from [55], Copyright (2019) American Chemical Society.

energy landscape sufficiently to suppress fast superspin relaxation, whereby the line ratio can again be extracted, reaching $A_{23(0.5\ T)} \approx 3.4$, corresponding to a low degree of orientation, matching the low Langevin parameter and high degree of surface spin canting expected for such small nanoparticles at moderate magnetic fields.

The observation of fast and beginning Néel relaxation in sample S and M, respectively, and blocked superspin relaxation in ferrofluid L was verified via detailed AC-susceptometry experiments as seen in Figure 8(b). Although for each individual sample only the dominant relaxation mechanism could be studied, values of the effective magnetic anisotropy in case of Néel relaxation in sample M from Mössbauer spectroscopy many-state relaxation modeling could be verified by this method, as well as the macroscopic dynamic viscosity of the carrier medium in sample L, where Brownian diffusion is the dominant process and results based on line broadening and particle rotation frequencies yielded matching viscosities.

5 Influence of matrix nanostructure on Brownian MNP motion

In discussions of magnetic hybrid materials, the interaction between the magnetic nanoparticles and the nanostructure of the surrounding matrix is essential and has not been covered in the previous chapters explicitly. To illustrate effects of the matrix properties on nanoparticle orientation and possible modes of motion, we study electrostatically stabilized spindle-shaped hematite nanospindles of ca. 387×85 nm. With an aspect ratio of ca. 4.5 the nanoparticles are expected to show distinctively anisotropic diffusion in fluid media, while also aligning perpendicular to external magnetic

fields due to their peculiar magnetic structure [56]. Here, they are dispersed in a precursor solution when polymerization starts, whereby the manifesting polymer network forms meshes around the nanoparticles, limiting their mobility to a certain degree. The degree of constriction in the PAAm-hydrogel depends on the network crosslinking density defined by the concentration c_{MBA} of N,N'-Methylene bis(acrylamide) (MBA) crosslinker in the range of 1.10^{-6} – 2.10^{-3} relative to the number of AAM monomers.

Dependent on the crosslinking, the hydrogels are widely tunable in their viscoelastic properties, with the "hardest" sample with highest c_{MBA} having a defined form and showing almost pure elastic response behavior, while the intermediate sample is softer and less resilient (Figure 9(b-d)). The "softest" hydrogel of minimum c_{MBA} is viscoelastic and easy to deform, with the ensemble of our hydrogel samples thereby covering a very broad range of macroscopic (visco-)elastic response behavior. While it stands to reason that hydrogels of lower crosslinking density and wider meshes will lead to less constraint of particle motion, the more important question is the following: What is the correlation between the probed mode of particle motion as well as the timescale of the experiment on the one hand, and the observed diffusive behavior on the other?

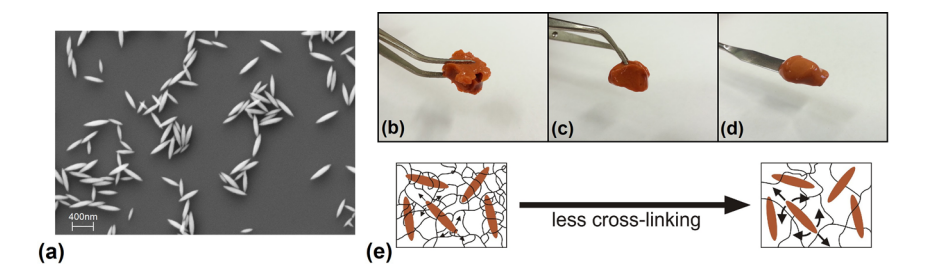


Figure 9: (a) SEM image of hematite nanospindles, and (b) hard, (c) medium and (d) soft hydrogel samples prepared using different crosslinking concentrations and (e) schematic illustration of increasingly free modes of particle motion. Adapted from [57] and with permission from [58] Copyright (2015) American Chemical Society.

Regarding this criterion, Mössbauer spectroscopy is a very local and relatively "fast" technique, meaning that even dynamic processes on the nanosecond timescale will produce considerable changes in spectral structure, while even slightly higher mean square displacements in atomic vibration/motion will yield far lower spectral intensity, as described by the Debye-Waller factor in Section 2. Both effects illustrate that via Mössbauer spectroscopy one will observe effects of particle-matrix interaction (if present) on very short time- and length scales. We should keep this in mind when studying the temperature-dependent line broadening of the three ferrohydrogels across their melting region. All samples have in common that instead of a sharply defined melting temperature we have a narrow region, in which the line broadening quickly increases before reaching the maximum value corresponding to the "liquid"

hydrogel state, with the steepest point of the curve being at almost identical temperatures T_{melt} for all samples. Linewidths in the liquid region above T_{melt} are in the range of 12–30 mm/s and increase for lower crosslinker densities. Although this was to be expected, the relatively low variation in linewidth is somewhat surprising, considering the significant differences in macroscopic viscoelastic behavior. But is there a measure or intuitive physical understanding, based on the observed decrease in line broadening, to which extent the particle motion is constricted? There are at least two states we can put these hydrogel results in relation to:

On the one hand a perfectly rigid surrounding matrix, allowing no additional atomic motion as compared to an atom in the crystal lattice of the immobile nanoparticle, which will yield the static linewidth Γ_{stat} , and on the other hand the state of motion undisturbed by the polymer network, in which the particles would exhibit free Brownian motion in water. For the latter, a simple estimation using Eq. (2.2) in case of spherical particles or a more precise estimation based on the direction-dependent diffusion coefficients of spindle-shaped nanoparticles yield a dynamic line broadening of ca. 400 mm/s, based on the viscosity of water $\eta_{RT} \approx 1$ mPas [59]. Compared to this wide spectrum of possible states of motion, values of Γ of the same magnitude seem to indicate similar degrees of constriction of translational nanoparticle diffusion, at least when studied on the short Mössbauer timescale.

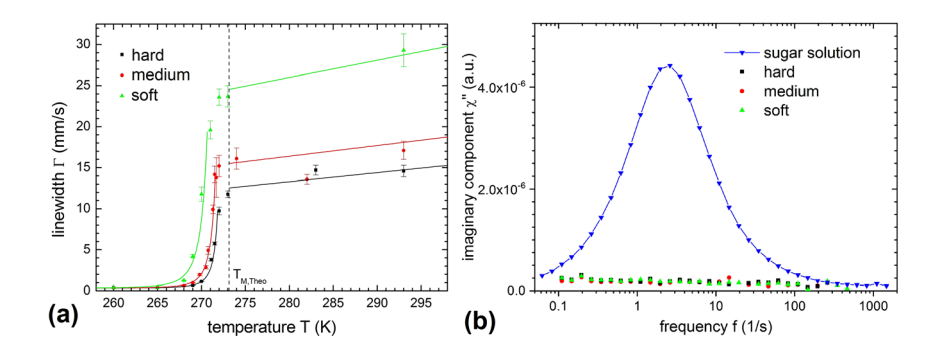


Figure 10: (a) Mössbauer absorption linewidth of hydrogels of different crosslinking density across the hydrogel melting region and (b) imaginary component of magnetic susceptibility of hydrogels compared to a 60 wt% sucrose reference solution, normalized to the concentration of included hematite nanospindles, adapted with permission from [58], Copyright (2015) American Chemical Society.

While in previous sections, AC-susceptometry provided reference values for individual samples, either in terms of Néel relaxation frequency or Brownian rotation frequency, here it is more essential to have it as a complementary technique, not only because of the much longer timescales that the particle dynamics are probed on. Of similar importance is the fact that via the combination of Mössbauer spectroscopy and AC-susceptometry, one has two techniques probing either translational or rotational

motion of the particles, which may experience widely different degrees of constriction, especially for the here studied anisotropic hematite nanospindles.

For that purpose, the imaginary part of magnetic susceptibility of a 60 wt% sucrose reference solution is shown in Figure 10(b). As expected, we find a distinct narrow peak at ca. 2–3 Hz, which would correspond to an effective particle radius in case of spherical particles of ca. 70–80 nm, using literature values of ca. $\eta_{300K} \approx 40$ mPas [60]. If particle rotation would not be hindered in the studied hydrogels, matching the free rotation in water, accordingly we would expect the peak to shift to higher frequencies by a factor of 40. Instead, no χ'' – signal is visible in the entire covered frequency range aside from a minor background almost independent of frequency. Reference experiments performed at different temperatures including the frozen hydrogel state (not shown) indicate that it can be assigned completely to Néel-type relaxation, presumably in the easy magnetic plane of the hematite nanospindles, in which magnetic reorientation can be induced even by very moderate thermal excitation due to its ultralow magnetic anisotropy [61, 62].

We would explain this apparent contradiction of our two experimental approaches regarding particle mobility either by the type of motion that is probed, or by the methods' timescales: Dependent on the timescale of network formation and crosslinking as compared to the particle diffusion coefficient, the hydrogel meshes will more or less reproduce the shape of the hematite nanospindles, with a minimum average distance between particle surface and polymer strings dependent on the crosslinker density. This very simple model does not consider friction induced by continuous direct contact between particles and the polymer network, which would equally hinder all types of motion. Nevertheless, it implies that while translational as well as rotational motion about the short particle axes are only possible on very short timescales before getting in contact with the constricting surrounding, particle rotation about the long axis should still be possible. This could indicate that it is less the probed mode of motion and more the timescale of the experiments which allows – or prevents – the detection of particle motion. As linewidths from Mössbauer spectroscopy, which are far lower than that of free particle motion, rather seem to indicate a constricted type of translational motion with slight variations in the degree of confinement, it seems reasonable that only on the very short timescales probed in Mössbauer spectroscopy the particles in average cover a distance short enough to not inevitably lead to contact with the polymer network. To verify this assumption, similar experiments with spherical particles could be helpful, where the hydrogels would presumably form isotropic meshes without preferred direction of motion, as well as a study of the mobility of particles in a nanostructured surrounding, whose length scale is independent of the used nanoparticles [17, 63].

6 Conclusion

Summarizing insights made for different magnetic hybrid materials, we find the main advantage of Mössbauer spectroscopy to be the ability to access a plethora of critical

system parameters simultaneously as it is shown in Figure 11, without the need to compare results recorded under different experimental conditions, although it should be mentioned that each parameter can be obtained individually at least with similar precision via a specialized complementary technique. The independence from sample transparency is also very helpful in combination with similar γ -ray absorption in water (ferrofluids), gels and many types of hydrocarbon-based systems (ferrogels and ferropolymers), covering most of the matrix materials currently used in the preparation of magnetic hybrid systems.

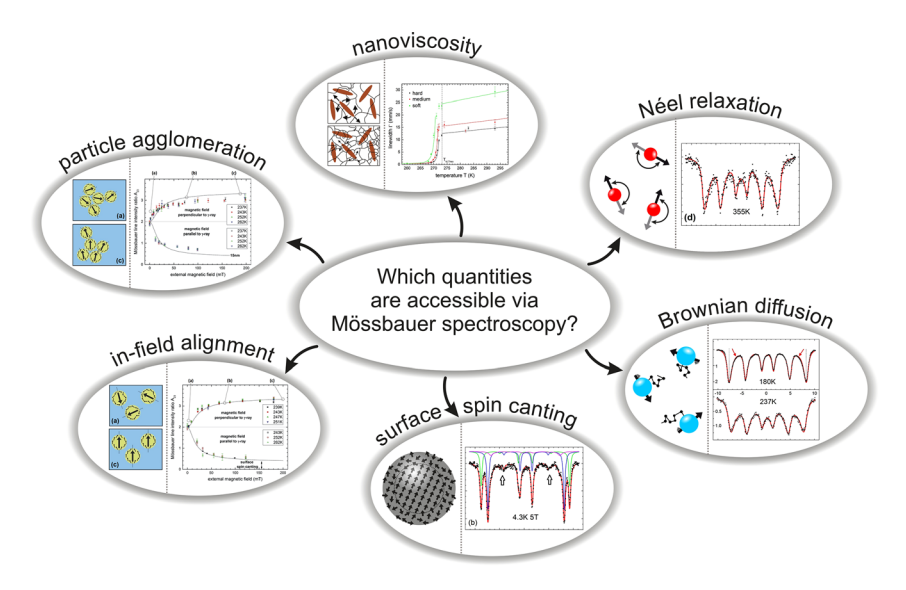


Figure 11: Quantities of interest in the study of magnetic soft hybrids via Mössbauer spectroscopy, adapted with permission from [19, 55, 58], Copyright (2015–2019) American Chemical Society, from [51], Copyright (2016), with permission from Elsevier and [57].

Apart from the experiments shown above, the special traits of Mössbauer spectroscopy could match specific problems perfectly, supporting future investigations of new hybrid materials. These include for example composites of magnetic nanoparticles and liquid-crystals as well as liquid-crystal elastomers, where the ability to probe particle diffusion and alignment at the same time may provide a better understanding of the interplay of magnetic particle dynamics with different self-ordered states of liquid crystal molecules. Connected to this, also the possibility of direction-resolved measurements of particle diffusion coefficients could be beneficial for studies on either anisotropic nanoparticles or particle diffusion in anisotropic surroundings. Similar to the field-dependent analysis of particle alignment presented in Section 4, Mössbauer experiments could be applied to analyze how nanoparticle chain formation behavior is affected by the nanostructure of surrounding matrix material, as chain

formation will affect the degree of magnetic alignment as well as the particle mobility. As it is common to apply external magnetic fields in Mössbauer spectroscopy, one could also think of researching the properties of actively heated MNPs in AC-fields, to support the development of better materials for magnetic hyperthermia. Further information regarding the correlation of magnetic and spatial particle orientation could be extracted, e.g., for α -Fe₂O₃ nanospindles as discussed in Section 5, utilizing effects of the electric field gradient in hematite.

Author contribution: All the authors have accepted responsibility for the entire content of this submitted manuscript and approved submission.

Research funding: This research was supported by the Deutsche Forschungsgemeinschaft (SPP 1681, project WE 2623/7).

Conflict of interest statement: The authors declare no conflicts of interest regarding this article.

References

- 1. Mössbauer RL. Kernresonanzfluoreszenz von Gammastrahlung in Ir¹⁹¹. Z Phys 1958;151:124–43.
- Barb D. Grundlagen und Anwendungen der Mössbauerspektroskopie. Berlin: Akademie-Verlag; 1980.
- 3. Klingelhöfer G, DeGrave E, Morris RV, Van Alboom A, de Resende VG, De Souza PA Jr., et al. Mössbauer spectroscopy on Mars: goethite in the Columbia Hills at Gusev crater. Hyperfine Interact 2005;166:549–54.
- 4. Schünemann V, Winkler H. Structure and dynamics of biomolecules studied by Mössbauer spectroscopy. Rep Prog Phys 2000;63:263–353.
- 5. Wagner FE, Kyek A. Mössbauer spectroscopy in archaeology: introduction and experimental considerations. Hyperfine Interact 2004;154:5–33.
- Concas G, Spano G, Cannas C, Musinu A, Peddis D, Piccaluga G. Inversion degree and saturation magnetization of different nanocrystalline cobalt ferrites. J Magn Magn Mater 2009;321:1893–7.
- 7. Bonchev T, Aidemirski P, Mandzhukov I, Nedyalkova N, Skorchev B, Strigachev A. A study of Brownian motion by means of the Mössbauer effect. Sov Phys JETP 1966;23:42–6.
- 8. Keller H, Kündig W. Mössbauer studies of Brownian motion. Solid State Commun 1975;16:253-6.
- 9. Singwi KS, Sjölander A. Resonance absorption of nuclear gamma rays and the dynamics of atomic motions. Phys Rev 1960;120:1093–102.
- 10. Anand HR, Mullen JG. Diffusion broadening of the Mössbauer line in Wüstite. Phys Rev B 1973;8: 3112–16.
- 11. Schwalbach P, Laubach S, Hartick M, Kankeleit E, Keck B, Menningen M, et al. Diffusion and isomer shift of interstitial iron in silicon observed via in-beam Mössbauer spectroscopy. Phys Rev Lett 1990;64:1274–7.
- 12. Knapp EW, Fischer SF, Parak F. The influence of protein dynamics on Mössbauer spectra. J Chem Phys 1983;78:4701–11.
- Parak F, Achterhold K, Schmidt M, Prusakov V, Croci S. Protein dynamics on different timescales. J Non-Cryst Solids 2006;352:4371–8.
- 14. Bonchev T, Vassilev I, Sapundzhiev T, Evtimov M. Possibility of investigating movement in a group of ants by the Mössbauer effect. Nature 1968;217:96–8.

- 15. Bhide VG, Kandpal MC. Mössbauer study of Brownian motion of FeSnO₃ particles in liquid-crystal N-(p-ethoxybenzylidene)-p'-butylaniline (EBBA). Phys Rev B 1979;20:85-90.
- 16. Nienhaus GU, Plachinda AS, Fischer M, Khromov VI, Parak F, Suzdalev IP, et al. Temperature dependence of the dynamics of ultrafine particles in a polymeric network. Hyperfine Interact 1990; 56:1471-6.
- 17. Plachinda AS, Sedov VE, Khromov VI, Suzdalev IP, Goldanskii VI, Nienhaus GU, et al. Mössbauer studies of bound diffusion in a model polymer system. Phys Rev B 1992;45:7716-23.
- 18. Gütlich P, Bill E, Trautwein AX. Mössbauer spectroscopy and transition metal chemistry. Heidelberg: Springer; 2011.
- 19. Landers J, Salamon S, Remmer H, Ludwig F, Wende H. Simultaneous study of Brownian and Néel relaxation phenomena in ferrofluids by Mössbauer spectroscopy. Nano Lett 2016;16:1150-5.
- 20. Ammar S, Jouini N, Fiévet F, Beji Z, Smiri L, Moliné P, et al. Magnetic properties of zinc ferrite nanoparticles synthesized by hydrolysis in a polyol medium. J Phys Condens Matter 2006;18: 9055-69.
- 21. Greneche J-M. Structural and magnetic properties of nanostructured oxides investigated by ⁵⁷Fe Mössbauer spectometry. Hyperfine Interact 2003;148/149:79-89.
- 22. Kodama RH, Berkowitz A, McNiff El Jr., Foner S. Surface spin disorder in NiFe₂O₄ nanoparticles. Phys Rev Lett 1996;77:394-7.
- 23. Mørup S, Topsøe H. Mössbauer studies of thermal excitations in magnetically ordered microcrystals. Appl Phys 1976;11:63-6.
- 24. Dormann JL, D'Orazio F, Lucari F, Tronc E, Prene P, Jolivet JP, et al. Thermal variation of the relaxation time of the magnetic moment of γ -Fe₂O₃ nanoparticles with interparticle interactions of various strengths. Phys Rev B 1996;53:14291-7.
- 25. Madsen MB, Mørup S, Costa TV, Knudsen JM, Olsen M. Superparamagnetic component in the orgueil meteorite and Mössbauer spectroscopy studies in applied magnetic fields. Nature 1986; 321:501-3.
- 26. Blume M, Tjon JA. Mössbauer spectra in a fluctuating environment. Phys Rev 1968;165:446-56.
- 27. Chuev MA. Mössbauer spectra of single-domain particles in a weak magnetic field. J Phys Condens Matter 2008;20:505201.
- 28. Jones DH, Srivastava KK. Many-state relaxation model for the Mössbauer spectra of superparamagnets. Phys Rev B 1986;34:7542-8.
- 29. Landers J, Stromberg F, Darbandi M, Schöppner C, Keune W, Wende H. Correlation of superparamagnetic relaxation with magnetic dipole interaction in capped iron-oxide nanoparticles. J Phys Condens Matter 2015;27:026002.
- 30. van Lierop J, Ryan DH. Mössbauer spectra of single-domain fine particle systems described using a multiple-level relaxation model for superparamagnets. Phys Rev B 2001;63:064406.
- 31. Heilmann I, Olsen B, Jensen JH. Non-Lorentzian diffusion-broadened Mössbauer lines. J Phys C Solid State Phys 1974;7:4355-60.
- 32. Elliott JA, Hall HE, Bunbury DS. Study of liquid diffusion by Mössbauer absorption and Rayleigh scattering. Proc Phys Soc 1966;89:595-612.
- 33. Dzyublik AY. Mössbauer effect in ellipsoidal Brownian particles. Sov Phys JETP 1974;40:763-5.
- 34. Steinmetz KH, Vogl G, Petry W, Schroeder K. Diffusion of iron in copper studied by Mössbauer spectroscopy on single crystals. Phys Rev B 1986;34:107-16.
- 35. Nack A, Seifert J, Passow C, Wagner J. Hindered nematic alignment of hematite spindles in poly(N-isopropylacrylamide) hydrogels: a small-angle X-ray scattering and rheology study. J Appl Crystallogr 2018;51:87-96.
- 36. Roeder L, Bender P, Kundt M, Tschöpe A, Schmidt AM. Magnetic and geometric anisotropy in particle-crosslinked ferrohydrogels. Phys Chem Chem Phys 2015;17:1290-8.

- 37. Brand RA, Hippert F, Frick B. Iron dynamics in Al-Cu-Fe quasicrystals and approximants: Mössbauer and neutron experiments. J Phys Condens Matter 2009;21:045405.
- 38. Keller H, Debrunner PG. Evidence for conformational and diffusional mean square displacements in frozen aqueous solution of oxymyoglobin. Phys Rev Lett 1980;45:68–71.
- 39. Żukrowski J, Błachowski A, Komędera K, Ruebenbauer K, Gabka G, Bujak P, et al. Dynamics of ternary Cu-Fe-S₂ nanoparticles stabilized by organic ligands. J Phys Chem C 2017;121:6977–85.
- Hansen MF, Morup S. Estimation of blocking temperatures from ZFC/FC curves. J Magn Magn Mater 1999;203:214–16.
- 41. Respaud M, Broto JM, Rakoto H, Fert AR, Thomas L, Barbara B, et al. Surface effects on the magnetic properties of ultrafine cobalt particles. Phys Rev B 1998;57:2925–35.
- 42. Webers S, Hess M, Landers J, Schmidt AM, Wende H. Effect of phase transitions in polymer solutions on the magnetic response of embedded nanoparticles. ACS Appl Polym Mater 2020;2: 2676–85.
- 43. Cherepanov VM, Gabbasov RR, Yurenya AY, Nikitin AA, Abakomov MA, Polikarpov MA, et al. Study of the Brownian broadening in the Mössbauer spectra of magnetic nanoparticles in colloids with different viscosities. Crystallogr Rep 2020;65:398–403.
- 44. Schröter K, Donth E. Viscosity and shear response at the dynamic glass transition of glycerol. J Chem Phys 2000;113:9101–9.
- 45. González JAT, Longinotti MP, Corti HR. The viscosity of glycerol-water mixtures including the supercooled region. J Chem Eng Data 2011;56:1397–406.
- 46. Segur JB, Oberstar HE. Viscosity of glycerol and its aqueous solutions. Ind Eng Chem 1951;43: 2117-20.
- 47. Müller R, Zhou M, Dellith A, Liebert T, Heinze T. Meltable magnetic biocomposites for controlled release. J Magn Magn Mater 2017;431:289–93.
- 48. Zhou M, Liebert T, Müller R, Dellith A, Gräfe C, Clement JH, et al. Magnetic biocomposites for remote melting. Biomacromolecules 2015;16:2308–15.
- 49. Müller R, Dutz S, Neeb A, Cato AC, Zeisberger M. Magnetic heating effect of nanoparticles with different sizes and size distributions. J Magn Magn Mater 2013;328:80-5.
- 50. Hansen MF, Koch CB, Mørup S. Magnetic dynamics of weakly and strongly interacting hematite nanoparticles. Phys Rev B 2000;62:1124–35.
- Müller R, Zhou M, Liebert T, Landers J, Salamon S, Webers S, et al. Mobility investigations of magnetic nanoparticles in biocomposites. Mater Chem Phys 2017;193:364–70.
- 52. Roca AG, Niznansky D, Poltierova-Vejpravova J, Bittova B, González-Fernández MA, Serna CJ, et al. Magnetite nanoparticles with no surface spin canting. J Appl Phys 2009;105:114309.
- 53. Gallagher KJ, Feitknecht W, Mannweiler U. Mechanism of oxidation of magnetite to γ -Fe $_2$ O $_3$. Nature 1968;217:1118–21.
- 54. Sidhu PS, Gilkes RJ, Posner AM. Mechanism of the low temperature oxidation of synthetic magnetites. J Inorg Nucl Chem 1977;39:1953–8.
- Landers J, Salamon S, Remmer H, Ludwig F, Wende H. In-field orientation and dynamics of ferrofluids studied via Mössbauer spectroscopy. ACS Appl Mater Interfaces 2018;11:3160–8.
- 56. Bødker F, Hansen MF, Koch CB, Lefmann K, Mørup S. Magnetic properties of hematite nanoparticles. Phys Rev B 2000;61:6826–38.
- 57. Landers J. Study of magnetic relaxation dynamics in soft matter nanoparticle composite systems [Dissertation]. Hrsg.: U. o. Duisburg-Essen; 2016.
- 58. Landers J, Roeder L, Salamon S, Schmidt AM, Wende H. Particle-matrix interaction in cross-linked PAAm-hydrogels analyzed by Mössbauer spectroscopy. J Phys Chem C 2015;119:20642–8.
- 59. Perrin F. Mouvement Brownien d'un ellipsoide (II). Rotation libre et dépolarisation des fluorescences. Translation et diffusion de molécules ellipsoidales. J Phys Radium 1936;7:1-11.

- 60. Rampp M, Buttersack C, Lüdemann H-D. Self-diffusion of sucrose in molasses. Ind Eng Chem Res 2000;39:4400-7.
- 61. Besser PJ, Morrish AH, Searle CW. Magnetocrystalline anisotropy of pure and doped hematite. Phys Rev 1967;153:632-42.
- 62. Flanders PJ, Remeika JP. Magnetic properties of hematite single crystals. Philos Mag A 1965;11:
- 63. Hess M, Roeben E, Rochels P, Zylla M, Webers S, Wende H, et al. Size effects on rotational particle diffusion in complex fluids as probed by magnetic particle nanorheology. Phys Chem Chem Phys 2020;16:7562-75.